JOURNAL OF MATERIALS SCIENCE **34** (1999) 3249–3261

Processing parameter effects on the reaction bonding of aluminum oxide process*

E. SUVACI, G. L. MESSING
Department of Materials Science and Engineering, Materials Research Laboratory, The Pennsylvania State University, University Park, PA 16802, USA
E-mail: messing@ems.psu.edu

The reaction bonding of aluminum oxide (RBAO) process was analyzed from the milling of the precursor mixtures to the sintering of the reaction bonded α-alumina as a function of precursor powder composition, Al particle size, temperature, and heating rate. The RBAO process involves both solid-gas ($T < T_{M,Al}$) and liquid-gas ($T > T_{M,Al}$) oxidation of $Al + \alpha$-Al_2O_3 powder compacts. It has been demonstrated that maximum Al content of the precursor powder is limited to 60 vol%. In addition, it was observed that the initial Al particle size affects the oxidation behavior significantly and hence final properties of α-Al_2O_3 compacts. Therefore, the initial Al particle size is very critical for the RBAO process. The critical Al particle size (i.e., the largest Al particle size can be used to obtain dense ceramic materials by the RBAO process) was determined as $\sim$1.5 μm. It has been demonstrated that heating rate can be used to improve the final microstructures of RBAO ceramics. Although there is no large (>4 vol%) amount of ZrO_2 addition, alpha aluminum oxide ceramics with 97% TD have been produced by optimizing the processing parameters such as fine (<1.5 μm) Al particles and slower heating rate during the liquid-gas oxidation.

1. Introduction

Reaction-based processing techniques have been gaining interest to form engineering ceramics and composites. Compared to conventionally processed ceramics, reaction based materials exhibit several advantages, including inexpensive raw materials, high stability, high purity and near net shape forming capability [1, 2]. Reaction based processing methods have been used successfully for the production of non-oxide ceramic materials (e.g., reaction bonded silicon nitride, reaction bonded silicon carbide) [3, 4]. However, the use of these methods to form oxide structural ceramics has only recently been reported. One of these methods is the DIMOX^{TM} process, developed by Lanxide in 1986 [5]. This process relies on the oxidation of molten Al in air at high temperatures. Since aluminum forms a stable oxide surface, alloying additives such as Mg, Si, and Zn have been added to molten aluminum to destabilize the protective oxide layer.

In 1989, another new technology, the reaction bonding of aluminum oxide (RBAO) process was introduced by Claussen *et al*. [6]. The reaction bonding process is also an oxidation based process which begins with a compact of aluminum and alpha alumina. During heating in air the Al particles are oxidized in the solid state at temperatures less than 660 °C, the melting point of Al, and then in the liquid state above 660 °C. The final product of the reaction bonding of the $Al + \alpha$-Al_2O_3 composite is monolithic α-Al_2O_3. Initial studies demonstrated a number of attractive characteristics of RBAO, such as high green strength, easy green machining, superior mechanical properties, near net shape capability (i.e., low shrinkage), broad microstructural and compositional versatility and inexpensive raw materials [7–13]. To date there are only a few papers about the fundamental nature of the process [14–16]. Therefore, the objective of this study was to develop a fundamental understanding of the RBAO process and from this understanding, to evaluate the effects of the processing parameters on the process. Thus, a series of experiments were conducted to investigate the effects of the initial composition, particle size and heating rate on the reaction bonding behavior of aluminum-alpha alumina powder mixtures.

2. Experimental

Different types of aluminum and alpha alumina powders were used to investigate the influence of the initial particle size on milling and reaction bonding. Two

* Presented at the 98th Annual Meeting of the American Ceramic Society, Indianapolis, IN, April 14, 1996 (Basic Science Division, Paper No. B-84-96).
Based in part on the thesis submitted by E. Suvaci for the M.S. degree in Materials Science and Engineering, Pennsylvania State University, University Park, PA, 1996.
Supported in part by Turkish Ministry of National Education.

TABLE I RBAO precursor powder compositions (vol %)

Raw materials	30A	45A	60A	80A	45B
VH-2 Al	30	45	60	80	—
ATA 105 Al	—	—	—	—	45
AKP50 Al_2O_3	70	55	40	20	—
Al4 Al_2O_3	—	—	—	—	55

commercial α-Al_2O_3 powders referred to as coarse ($\sim$6–10 μm, A14 Low soda alumina, Alcoa Chemical Co., Bauxite, AR 72011) and fine ($\sim$0.2 μm, AKP-50 High Purity Alumina, Sumitomo Chemical Co., Ltd., Tokyo, Japan) and two commercial Al powders, ATA-105 (5–50 μm Atomized Aluminum Powder, Alcan-Toyo America, Inc., Naperville, IL 60563) and VH-2 (2–5 μm Atomized Aluminum Powder, Valimet, Inc., Stockton, CA 95206), were studied. No dopants were added. The mixtures studied are listed in Table I. The notation for the compositions gives the volume percent Al and a letter defining which powder combination was used to prepare the mixtures before milling. The letter A represents the combination of fine alpha alumina and VH-2 aluminum powders and B represents the coarse alpha alumina and ATA-105 powder mixture.

After the aluminum and alpha alumina particles were mixed, the powder mixtures were attrition milled to reduce the particle size and increase homogeneity. For the grinding experiments 70% of the 600 ml stainless steel grinding container was filled with 4 vol % powder, 36 vol % milling liquid (i.e., isopropanol) and 60 vol % milling balls. Polyurethane agitator discs were used to reduce contamination during the milling. The precursor powder mixtures 30A, 45A, 60A, and 80A were milled with 0.5 cm diameter high purity alpha aluminum oxide balls (Diamonite, Shreve, Ohio) at 2000 rpm for 1 h. The 45B series was milled with 0.1 cm diameter yttria stabilized tetragonal zirconia (YTZ) balls at 2000 rpm. The degree of milling was varied by changing the milling time from 1 to 4 h for the 45B powder compositions. Consequently, only the A series was used to investigate the effects of the initial composition on the RBAO process. The 45B powder compositions were used mainly to determine the effects of Al particle size and heating rate on the process. To determine the amount of contamination from the milling balls, the milling media were weighed before and after the milling process. Since the intense milling action produces considerable heat, a water cooling system was used to control and keep the slurry temperature low during the milling process.

The particle size distribution of the milled powder mixtures was determined by laser light scattering (SALD 2001, Shimadzu Scientific Instruments, Inc., Columbia, MA 21046). Milled powders were dried in a rotary evaporator (Model RE-51, Yamato Rotary Evaporator). Dried powders were sieved to $<$90 μm to eliminate large agglomerates in the mixture. The sieved powder was uniaxially pressed at 30 MPa in a stainless steel die to obtain 1.21 cm diameter and 0.22 cm high pellets. The pellets were then cold isostatically pressed for 5 min (Isostatic Press, Autoclave Engineers, Erie, PA) at pressures from 56 to 280 MPa to obtain the same relative green density for different compositions.

To characterize the reaction temperatures during reaction bonding, differential thermal analysis (DTA, Model 1600 DTA, TA Instruments 2100, Newcastle, DE) was performed for each composition. In addition, thermogravimetric analysis data were used to monitor the degree of oxidation. The pellets were reaction bonded at 3 different temperature regimes: (i) solid-gas (450–660 °C), (ii) liquid-gas (660–1100 °C), and (iii) sintering (1100–1600 °C). In the first temperature regime, two heating rates, 0.5 and 5 °C/min, were used to investigate the effect of heating rate on the solid-gas oxidation reaction. The pellets were reaction bonded at 620 °C for 2 h to evaluate the physical and chemical properties of samples in the solid/gas temperature range. In the second temperature regime, one heating rate, 5 °C/min, was used and the pellets were reaction bonded at 730, 900, 1000, and 1130 °C to examine how the physical and chemical properties of the samples change during the liquid/gas oxidation reaction. In the third temperature regime, sintering was performed in a high temperature furnace. The reaction bonded pellets were sintered from 1200 to 1600 °C for 2 h. The densities of the pressed pellets were determined by the dimensional method, and densities of the reaction bonded and sintered pellets were determined by the Archimedes' technique.

The degree of reaction data obtained from thermogravimetric analysis was verified by qualitative XRD (Model RU271019A, Rigaku Co., Tokyo, Japan). Thermomechanical analysis (TMA, TMA-50 Thermomechanical Analyzer, Shimadzu Corp., Kyoto, Japan) was used to monitor the dimensional changes during reaction bonding and sintering. Scanning electron microscopy (SEM, Model ISM 6300 JEOL, Tokyo, Japan) was used to examine the microstructural development during reaction bonding and sintering.

3. Results and discussion

3.1. Processing

3.1.1. Milling and compaction

The reaction bonding of aluminum oxide (RBAO) process begins with a milling operation. Attrition milling is generally the preferred method for comminution due to its high milling efficiency [17]. During attrition milling, some amount of wear debris from the milling balls is observed in the slurry. In all cases examined there was about 0.3–0.8 wt % wear debris from the milling balls. After 1 h milling of the 45B powder there was $\sim$0.3 wt % wear debris from the YTZ balls and $\sim$0.6 wt % wear debris from the alpha alumina balls. In addition it was observed that the amount of wear debris decreases as the aluminum content increases in the initial mixture.

Fig. 1a and b show the particle size distributions of the 45B powder after 1 and 4 h milling, respectively. Since the initial α-Al_2O_3 particles are $<$10 μm, the particles $>$10 μm are the Al particles. After 4 h milling the particle size of the mixture is reduced, and the particle size distribution shows a trimodal character. After 4 h milling the 45B powder was determined by SEM and EDS to consist of fine and flaky Al particles, and coarse and tabular α-Al_2O_3 particles (Fig. 2). Therefore, in

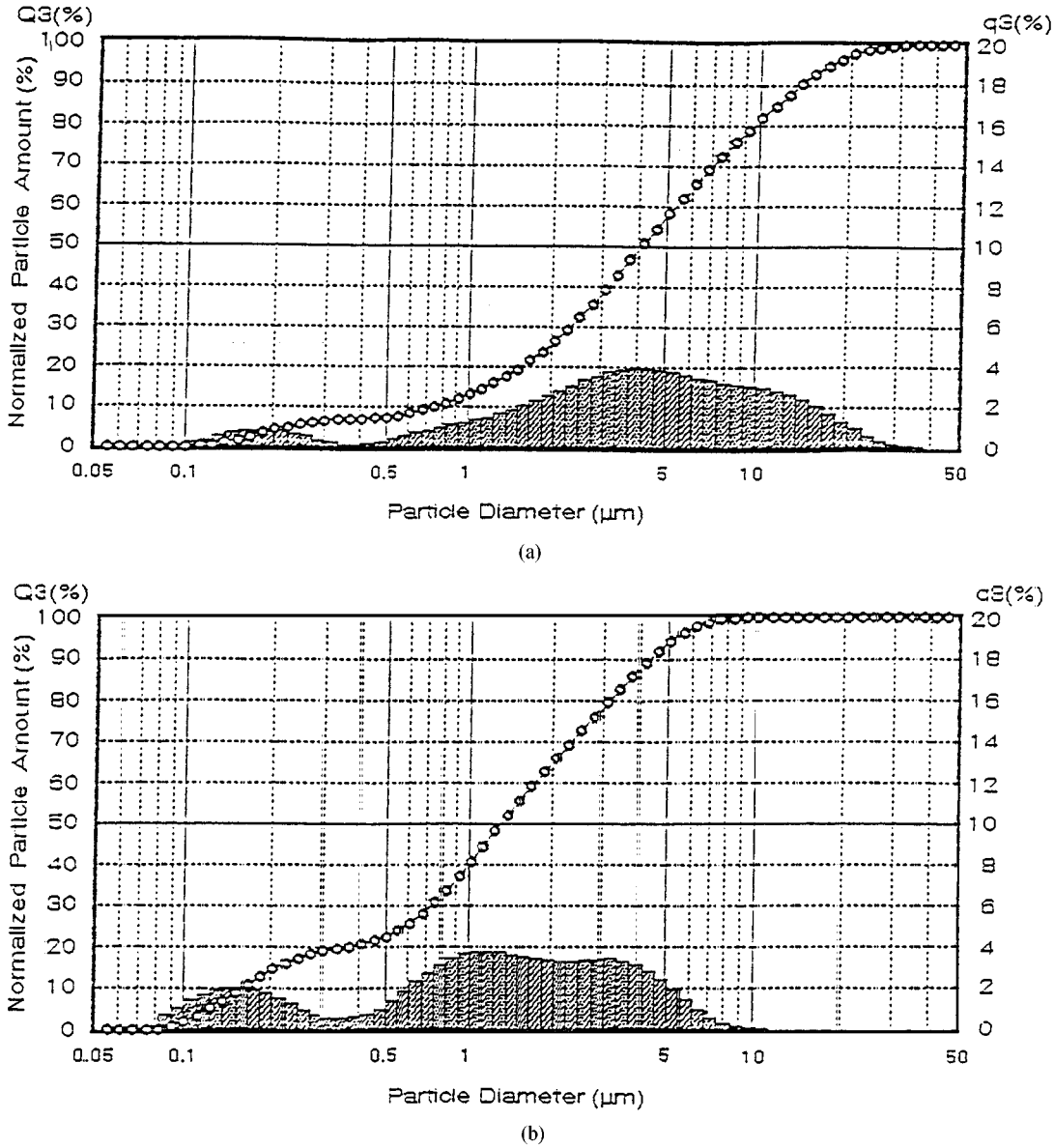

Figure 1 The particle size distributions of the 45B powder after (a) 1 and (b) 4 h milling with 1 mm YTZ balls.

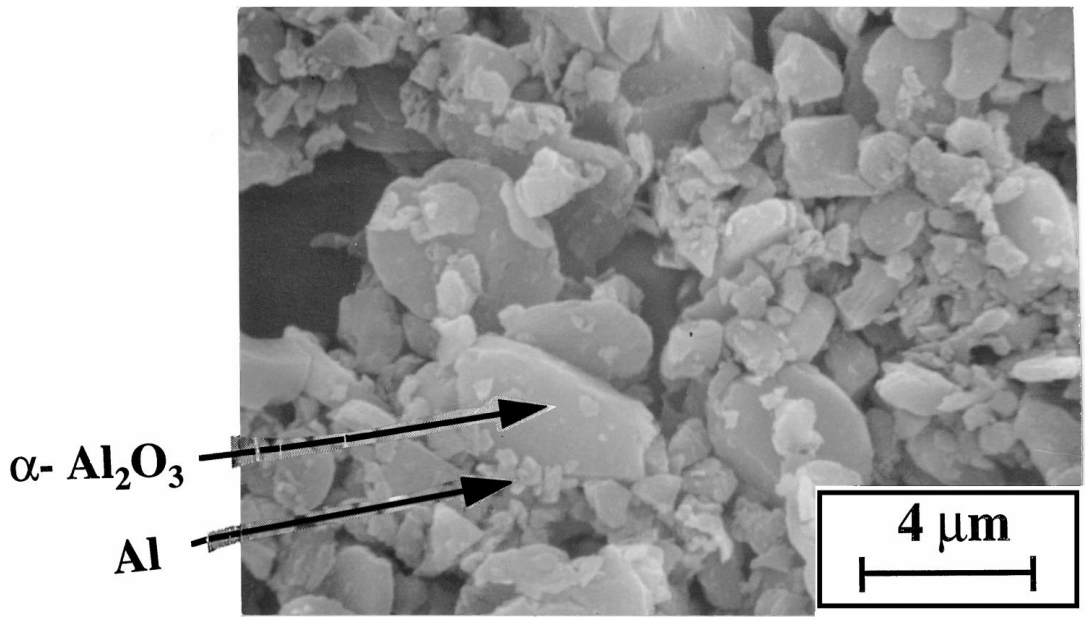

Figure 2 SEM micrograph of the 45B powder after 4 h milling with 1 mm YTZ balls.

Fig. 1b most of the large particles (>1.5 μm) are α-Al_2O_3 particles. Particles 0.5–1.5 μm in size are Al particles and fine particles (<0.5 μm) are a mixture of α-Al_2O_3 and Al particles. This means that after 4 h milling the Al particle size is reduced to <1.5 μm.

In addition to particle size reduction, it was observed that some of the initial Al oxidized during milling. As determined by TGA, 3 wt % of the initial Al in the 45B powder oxidized, after 1 h and 21 wt % of the initial Al oxidized after 4 h (Fig. 3). The XRD patterns of the ATA-105 Al powder milled for different times are shown in Fig. 4. The decrease in the Al peak intensities is due to Al oxidation during milling. The ZrO_2 wear debris could not be observed by XRD. This may be due to the peak broadening caused by the lattice distortion of tetragonal zirconia during milling [18]. After heating the powder to 730 °C in air, the tetragonal zirconia peaks appeared in the XRD pattern (Fig. 5B).

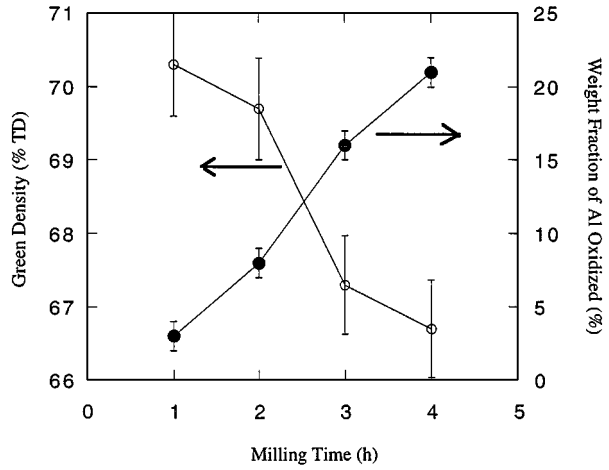

Figure 3 The dependence of green density and oxidation of initial Al in the 45B powder mixture on milling time (compaction pressure: 280 MPa).

The theoretical densities of the three-phase green compacts were estimated by the rule of mixtures, using 3.986, 2.7, and 3.0 g/cm^3 [19] for the theoretical densities of alpha alumina, aluminum and amorphous alumina, respectively. Fig. 6 shows the relative green densities for different compositions of the RBAO precursor powder as a function of compaction pressure. The relative green densities increase with increasing compaction pressure for all compositions. Since Al is ductile, increasing the Al content in the initial powder mixture results in higher relative green densities with increasing compaction pressure. The 30A samples were ~65% dense after isostatic compaction at 280 MPa. The 45A samples isostatically pressed at 280 MPa were ~71% dense. The 45B samples showed different relative green densities after isostatic compaction due to the different milling times. The dependence of relative green density on milling time is shown in Fig. 3 for these samples. The samples milled for one

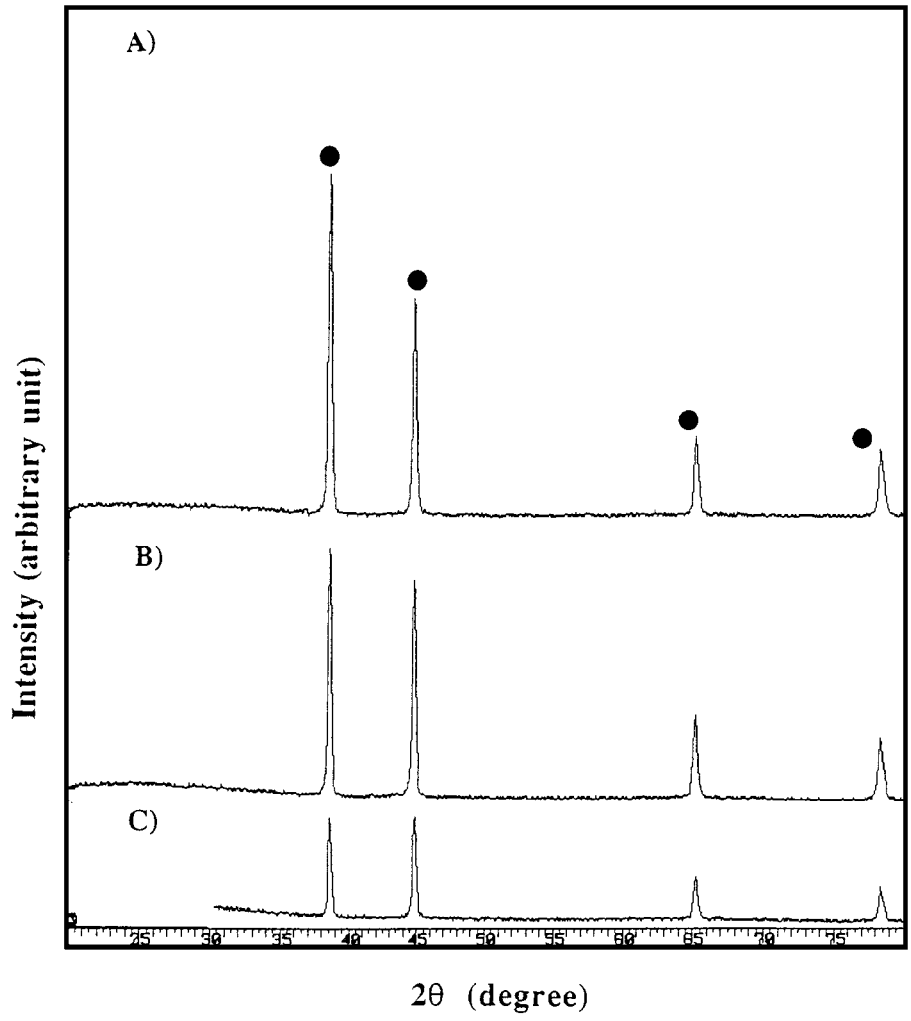

Figure 4 The XRD patterns of ATA-105 Al powder after (A) 2, (B) 3, and (C) 5 h milling with 1 mm YTZ balls (● aluminum).

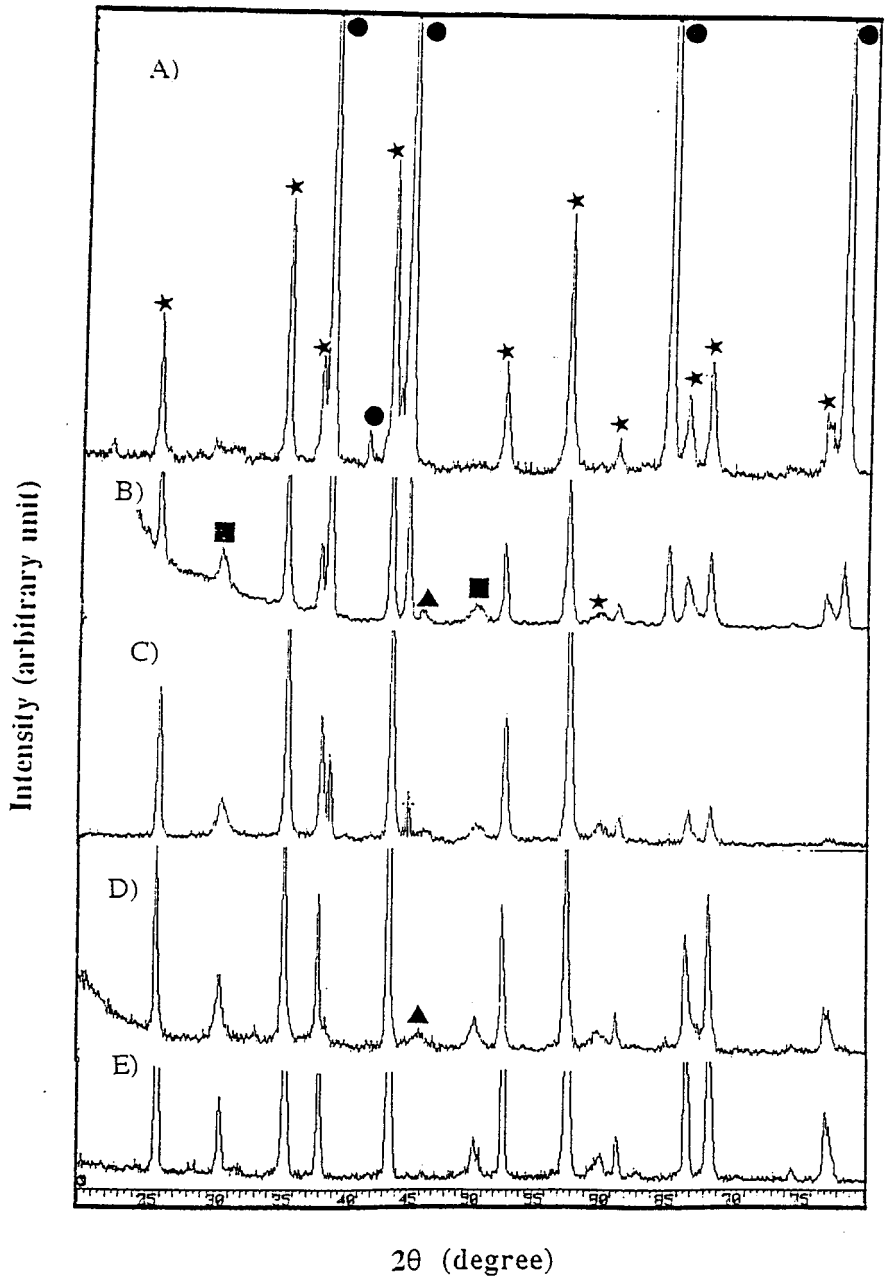

Figure 5 The XRD patterns of the 45B samples after (A) 1 h milling, and reaction bonding at (B) 730, (C) 900, (D) 1130, and (E) 1200 °C for 1 min (● aluminum, ∗ alpha alumina, ▲ gamma alumina, ■ tetragonal zirconia).

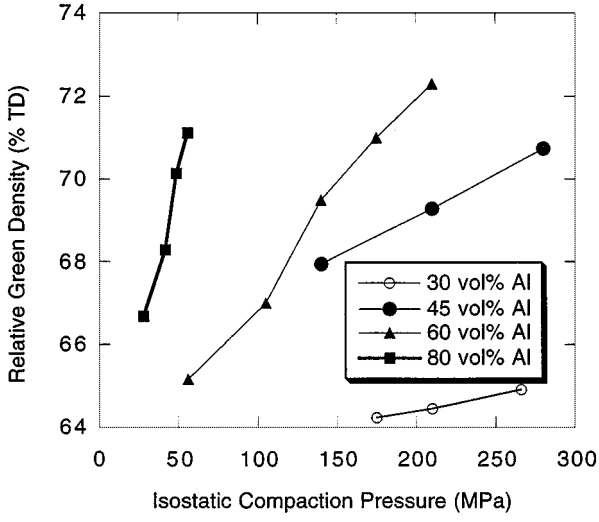

Figure 6 The dependence of relative green density on isostatic compaction pressure and initial powder compositions which were milled for 1 h with 5 mm alpha alumina balls.

hour exhibited 70.3 ± 1.0% relative green density and the samples milled for four hours were 66.7 ± 1.0% relative green density. This result can be attributed to the decrease in the Al content by oxidation during the milling.

3.1.2. Reaction bonding and sintering

Samples with a relative green density of 68.5 ± 1.0% TD were selected for the reaction bonding experiments. The 45B samples which were milled for 1 h were selected as a model system because most of the compositions show similar reaction bonding and sintering behavior except for the 4 h milled 45B powders. The reasons for the differences will be discussed later. TGA and DTA (Fig. 7) show that there is no significant weight change and reaction up to 450 °C. The TMA (Fig. 8) data shows only a small dimensional change below 450 °C. These results indicate that the aluminum

oxidation rate is near zero below this temperature. This conclusion is consistent with reports that the slow oxidation of Al is controlled by Al^{+3} ion diffusion through the protective aluminum oxide surface layer below 450 °C [20].

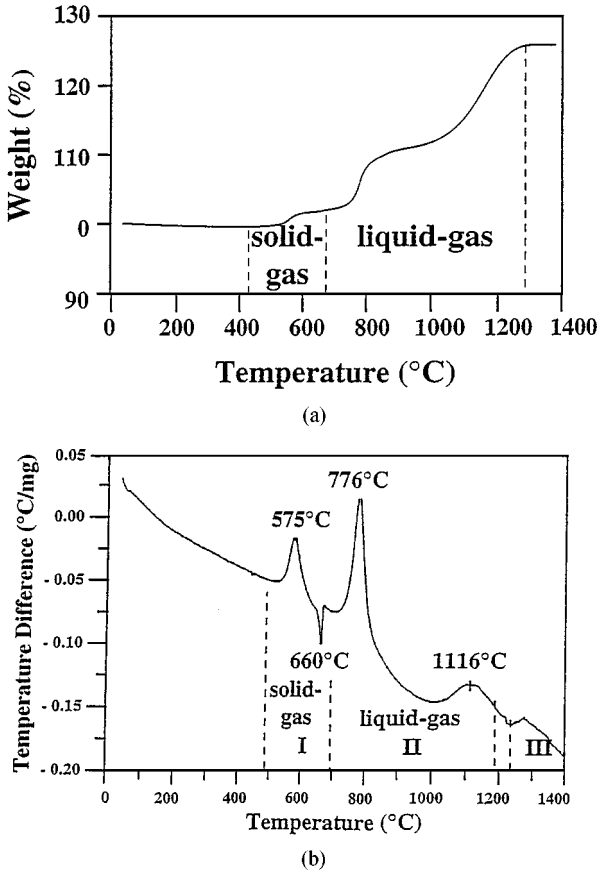

Figure 7 (a) Thermogravimetric and (b) differential thermal analyses of the 45B samples which were compacted at 210 MPa after 1 h milling and heated at 5 °C/min.

Above 450 °C, the oxidation rate increases as demonstrated by the weight gain and the increased slope in the TMA curve. The DTA curve also shows a highly exothermic reaction at ∼575 °C and consistently, the slopes in the TGA and TMA data indicate the maximum reaction rate at 575 °C. This significant increase in oxidation rate can be caused by acceleration of the frequency of ruptures of the oxide film as a result of reduction in its mechanical strength. V. G. Shevchenko *et al*. reported that a significant increase in oxidation rate can be caused by the increase in the diffusion rate of ions through the protective layer at the moment of rearrangement of the oxide structure [21]. Between 575 and 660 °C the reaction rate decreases as a result of the formation of a protective aluminum oxide surface. For the 45B samples, milled for 1 h and heated at 5 °C/min, 11% of the Al oxidized to Al_2O_3 below 660 °C.

The melting of Al at 660 °C results in a 14% increase in volume as a result of the specific volume difference between solid and molten Al. Melting is evidenced in the TMA curve as a steep deflection and in the DTA curve as an endothermic reaction peak. According to the XRD data in Fig. 5B, γ-Al_2O_3 is the only oxidation product at 730 °C. Heating above 725 °C leads to a marked increase in the oxidation rate and increase in the sample dimensions. This reaction reaches a maximum rate at 776 °C. Between 850 and 1050 °C, the oxidation rates decreases, again. During this initial liquid/gas oxidation stage, 30% of the Al is oxidized in the 45B samples milled for 1 h.

The exothermic peak in the DTA curve at 1116 °C indicates a late liquid/gas oxidation reaction. TMA and TGA data also show this reaction results in an increase in dimensions and a weight gain at about 1116 °C, respectively. The XRD pattern of the sample shows that the oxidation product is γ-Al_2O_3 at 1130 °C (Fig. 5D). The decrease in the sample dimensions at 1164 °C is

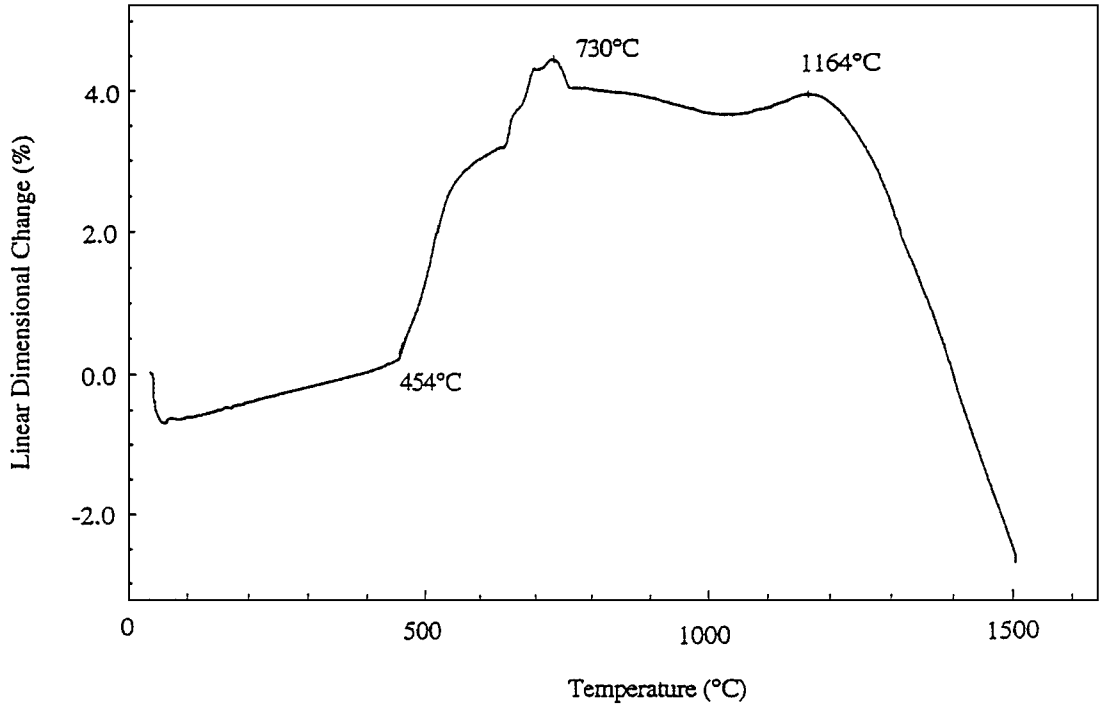

Figure 8 Thermomechanical analysis of the 45B samples which were compacted at 210 MPa after 1 h milling and heated at 5 °C/min.

attributed to transformation of gamma alumina to alpha alumina and the associated specific volume decrease of 20%. XRD of the samples reaction bonded at 1200 °C show only α-Al_2O_3 and tetragonal zirconia peaks (Fig. 5E). During the late oxidation stage, 59% of the total Al oxidation occurred for the 45B samples which were milled for 1 h. For the 45B samples with 3 h milling time, only ~2% of the total Al oxidation occurred during the late oxidation stage. The DTA and TMA data of the 45B samples after 4 h milling are given in Fig. 9. As seen from these data sets the oxidation reaction is complete at about 1050 °C for these compacts. Therefore, the occurrence of late stage oxidation is attributed to oxidation of large Al particles (>1.5 μm).

At 1200 °C the reaction bonded α-Al_2O_3 begins to sinter for the 45B samples which were milled for 4 h. As shown in Fig. 10, the late stage oxidation behavior, indicated by an increase in dimensions is observed for the 1, 2, and 3 h milled samples between 1100 and 1200 °C. Samples with longer milling times exhibited less amount of expansion between 1100 and 1200 °C.

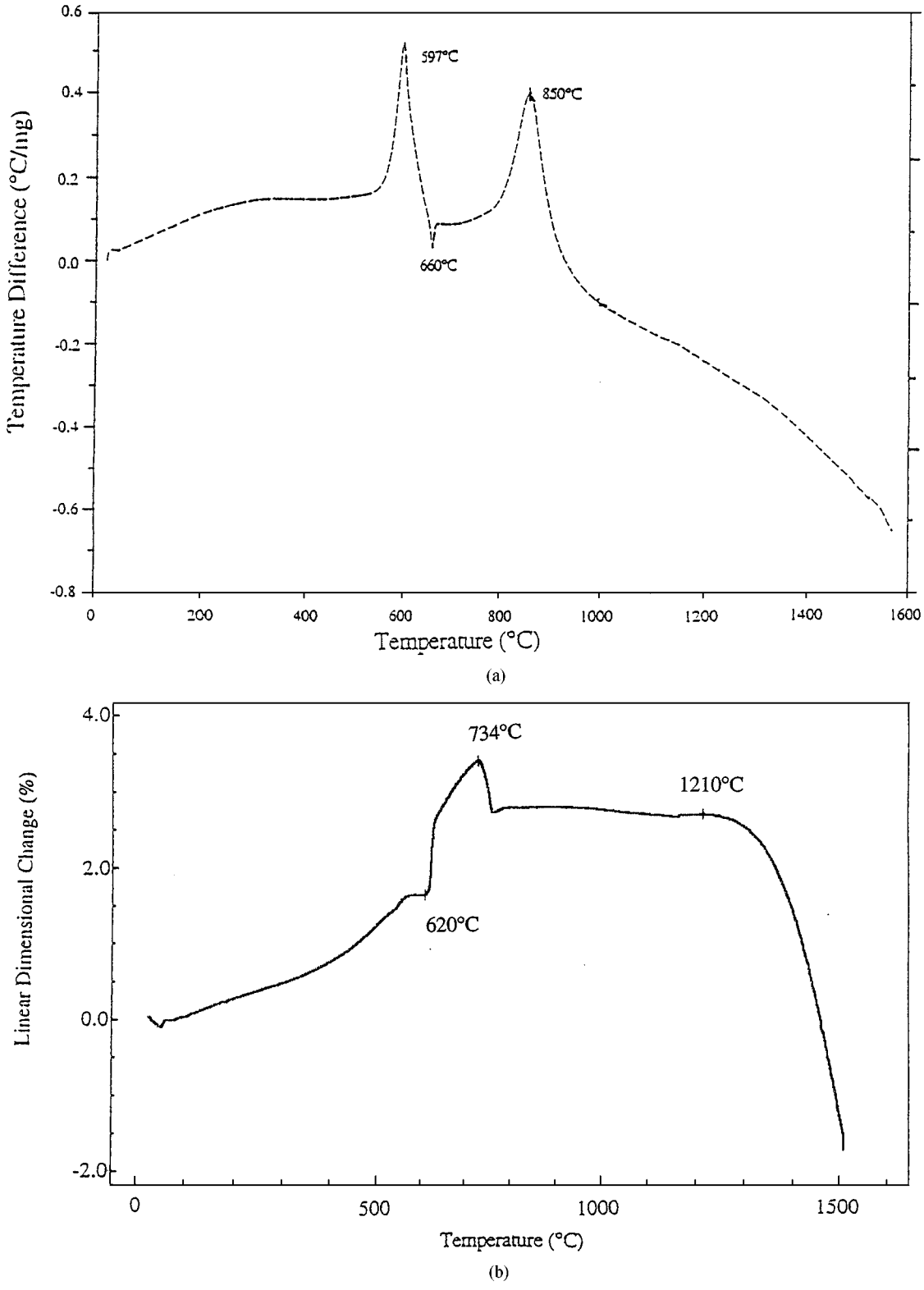

Figure 9 (a) Differential thermal and (b) thermomechanical analyses of the 45B samples which were compacted at 280 MPa after 4 h milling and heated at 5 °C/min.

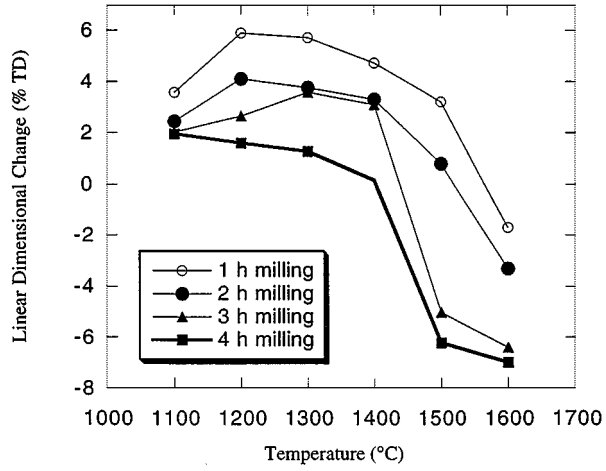

Figure 10 The dimensional changes during sintering as a function of sintering temperature.

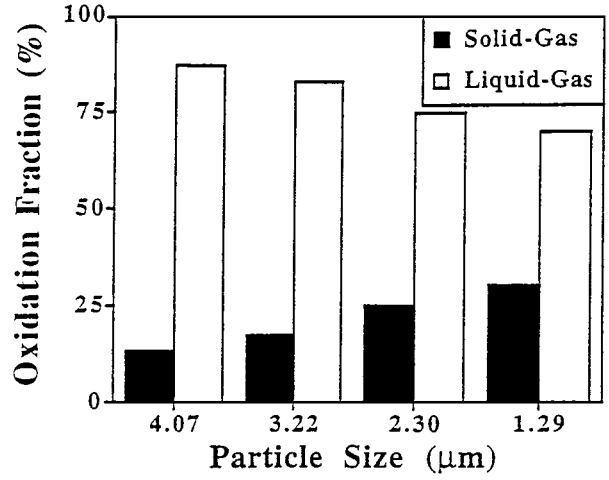

Figure 12 The effect of particle size on the reaction type for the 45B samples which were heated at 5 °C/min.

Since the 4 h milled samples have the highest final relative density (i.e., 94% TD), they show the largest dimensional change (−7%). However, even this value is less than the shrinkage which conventionally processed powders would exhibit. In the fully reacted body 'new' α-Al_2O_3 grains, formed from Al powders, and 'old' α-Al_2O_3 grains, from the precursor powder mixture, coexist. Since the initial α-Al_2O_3 particle size is relatively larger than α-Al_2O_3 grains formed from Al powders, grain size distribution exhibits a bimodal character.

3.2. Effect of processing parameters

3.2.1. Initial composition

The initial composition of the RBAO precursor powder mixture is an important processing parameter because it affects each subsequent processing step involved in the evolution of the RBAO-derived alumina. To determine the effect of the Al content on the reaction bonding process, 3 sets of samples with the same

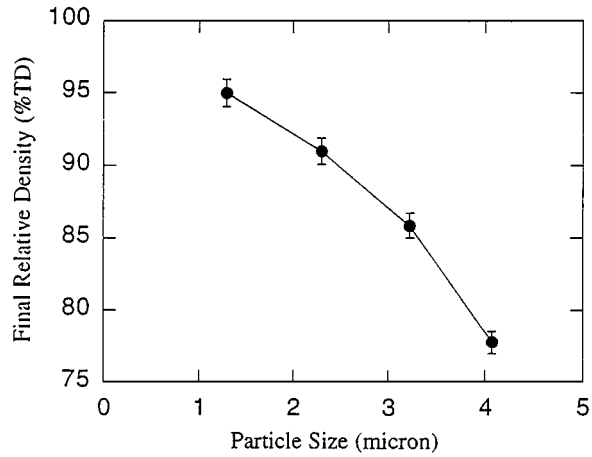

Figure 13 The effect of particle size on the relative densities of the 45B samples which were heated at 5 °C/min and sintered at 1600 °C for 2 h.

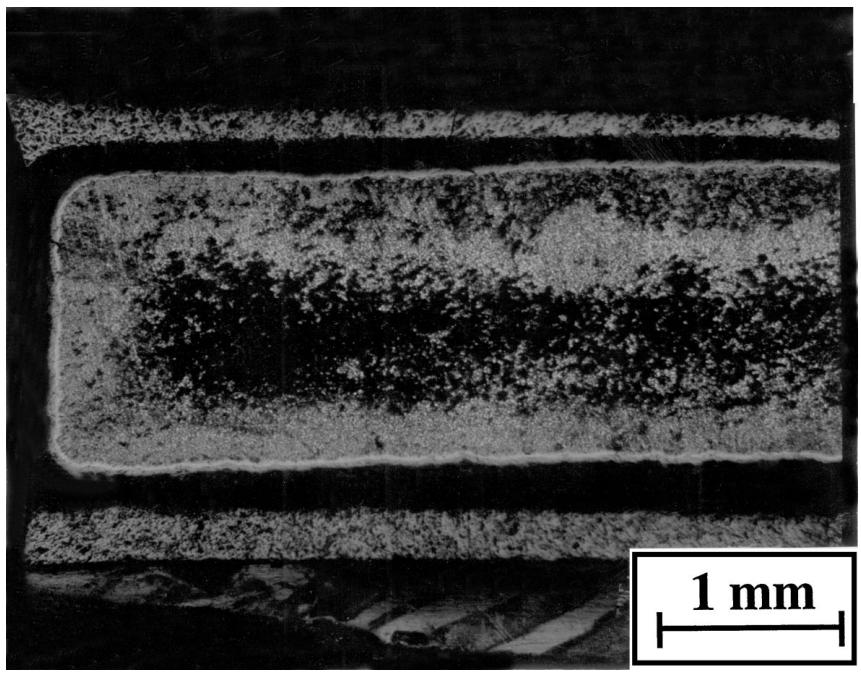

Figure 11 Optical micrograph of the 80A sample which was heated at 5 °C/min and sintered at 1600 °C for 2 h.

green density ($68.5 \pm 1.0\%$ TD) were heat treated at the same condition. The compositions of the precursor powder mixtures were chosen to investigate the limits of the initial Al content for the RBAO process. The powders, 45A, 60A, and 80A were milled for 1 h and then heated at 5 °C/min and sintered at 1600 °C for 2 h. Although there were no visible cracks in the samples, several small Al spheres were observed on the sample surfaces. The size and the amount of the Al spheres on the sample surface increase with increasing Al content in the precursor powder. Holz *et al*. reported that the size of the Al spheres also increases with increasing compaction pressure [16]. A black core consisting of Al still remains in the center of the 80A sample (Fig. 11). In contrast, other samples, 45A and 60A, were completely oxidized; similar results were observed with slow heating rate (i.e., 0.5 °C/min). It appears that a large amount of Al (>60 vol %) is problematic. The oxidation starts from the surface and forms an aluminum oxide crust. Once this crust starts to sinter, oxygen diffusion into the system becomes very slow. Although the 45A and 60A samples were completely oxidized, they exhibited low final densities. At the end of the process the 45A samples were 85% dense and the 60A samples were 78% TD. This difference may be attributed to the larger amount of Al (∼75%) oxidized in the late liquid/gas oxidation stage (i.e., above 1100 °C) for 60A samples than that of 45A samples (∼55%). These results indicate that the initial composition is a critical processing parameter and the maximum initial Al content for Al-α-Al_2O_3 system is 60 vol % to obtain dense ceramic materials.

3.2.2. Particle size

Since the RBAO process is an oxidation process, the particle size of the reactive constituent of the mixture (i.e., Al) is expected to affect the reaction bonding behavior of the compacts. Wu and Holz reported that to obtain dense RBAO ceramics the initial Al particle size should be less than 1 μm [14, 16]. However, they did not report any data which shows how they calculated this critical particle size. When the reaction bonding behavior of the powders with different milling times

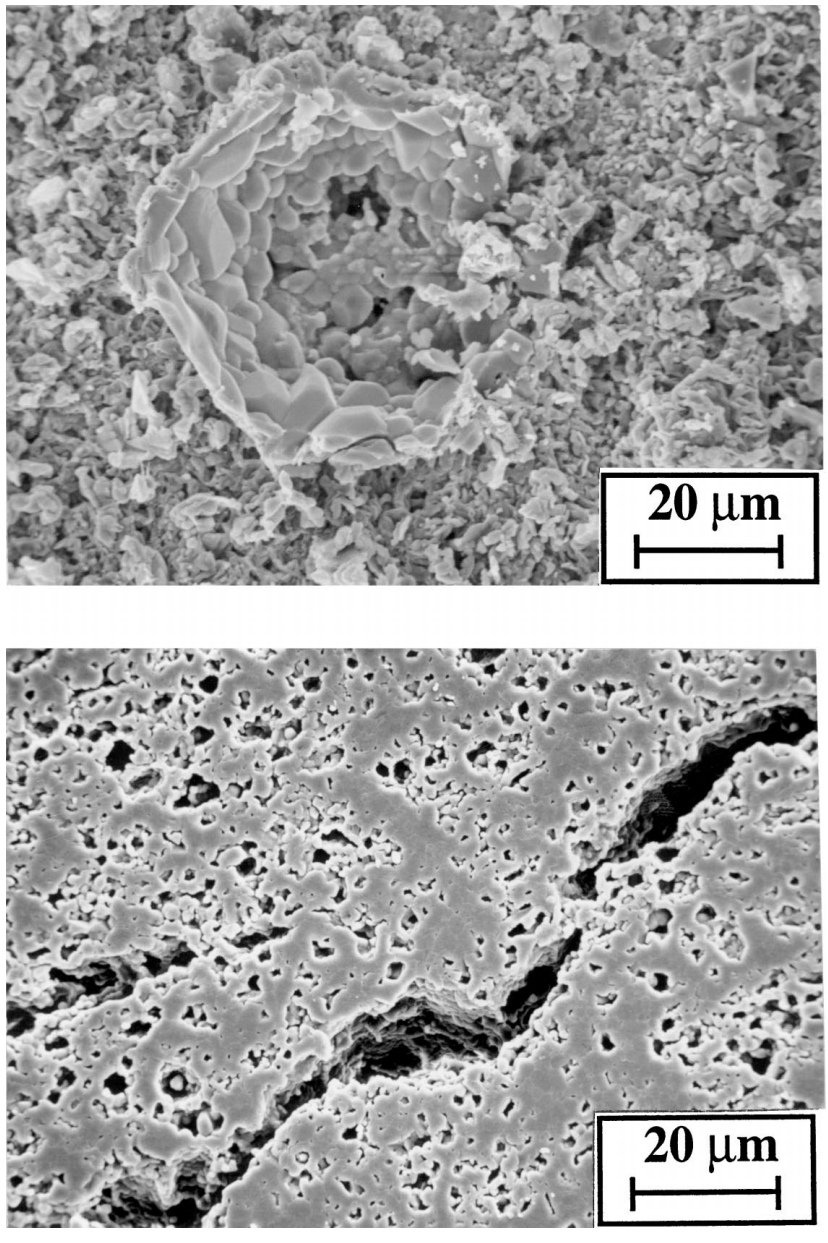

Figure 14 Molten Al leads to large pores and cracks in the reaction bonded compacts.

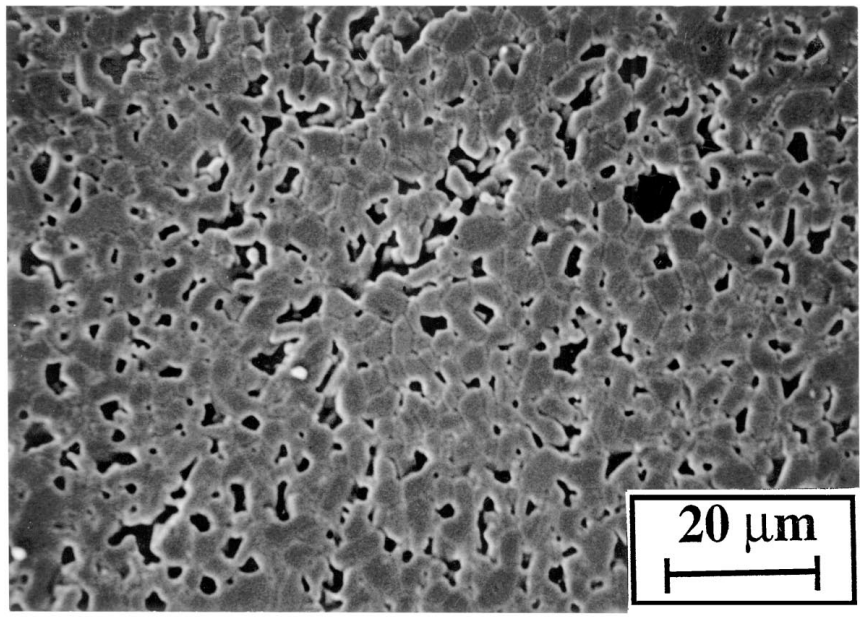

(a)

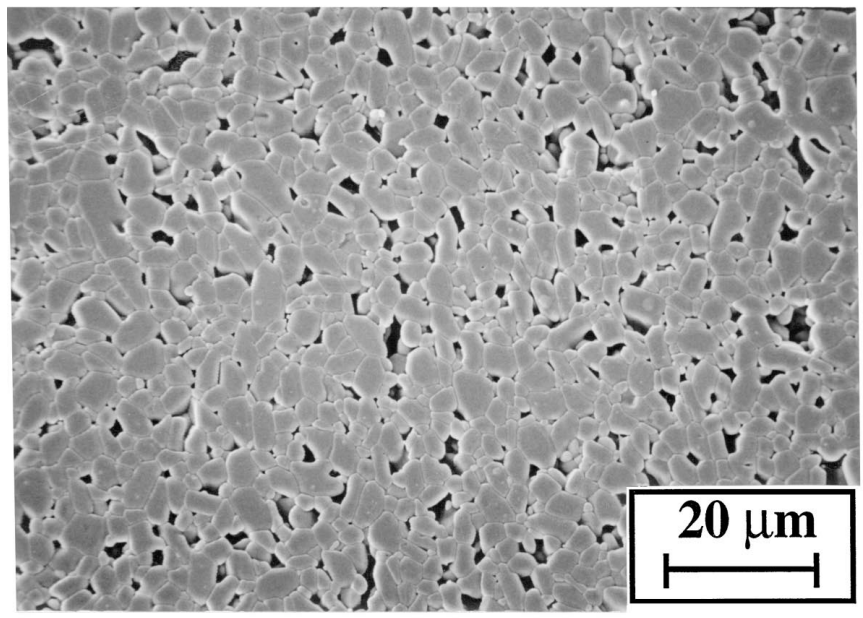

(b)

Figure 15 SEM micrographs of the 45B samples which were heated at 5 °C/min and sintered at 1600 °C after milling for (a) 1, (b) 2, (c) 3, and (d) 4 h. (*Continued.*)

are compared, it is concluded that decreasing particle size increases the solid/gas to liquid/gas ratio as shown in Fig. 12. For the 45B compacts containing large Al particles (>1.5 μm) the solid/gas to liquid/gas ratio was 11/89 and for the 45B compacts containing fine Al particles (<1.5 μm) this ratio was 34/66 at 5 °C/min. The final relative densities of the 45B powder samples, reaction bonded and sintered at 1600 °C for 2 h as a function of particle size of the mixture, are given in Fig. 13. The 45B compacts, containing large Al particles (>1.5 μm), exhibited lower final densities than the 45B compacts containing small Al particles (<1.5 μm). According to these results, decreasing the Al particle size increases the final relative density. It seems that the low final densities are a result of formation of the liquid phase (molten Al) in the system. It should be noted that the melting of Al is accompanied by a 14% volume increase. Therefore, at temperatures above 660 °C, molten Al droplets coagulate and, due to poor Al wetting on α-Al_2O_3, the droplets are squeezed out of body along the open pore system. During this process, migration of molten Al leads to large voids and cracks as shown in Fig. 14.

As shown in Fig. 15a these large voids and cracks are observed in the final structure as large pores and flaws. As the Al particle size decreases, the portion of these pores and flaws in the structure decreases (Fig. 15). The 45B samples containing fine Al particles (<1.5 μm) did not exhibit any of these types of defects after reaction bonding and sintering at 1600 °C for 2 h (Fig. 15d). These results demonstrate that the particle size of the RBAO precursor powder is one of the most important processing parameters. Since Al is the reactive constituent of the mixture, the Al particle size is especially

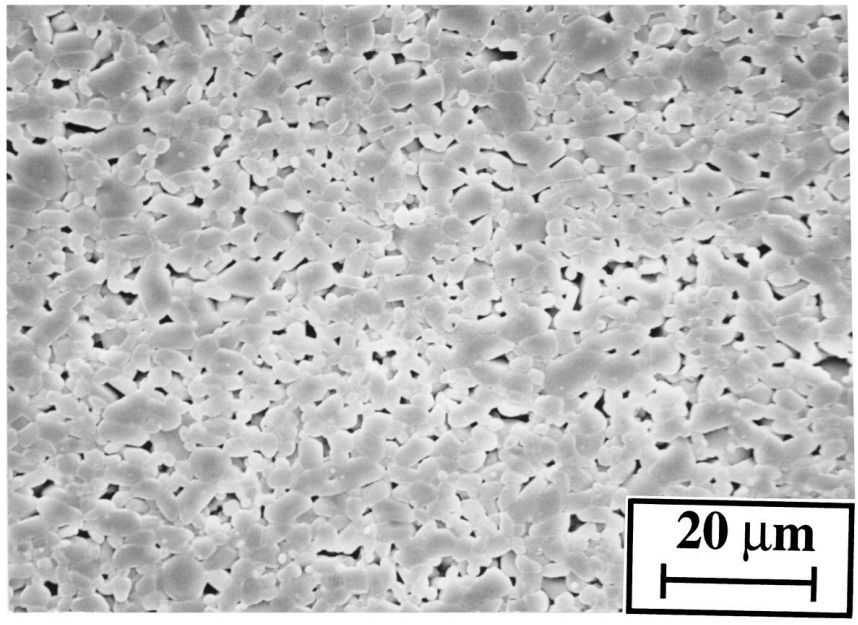

(c)

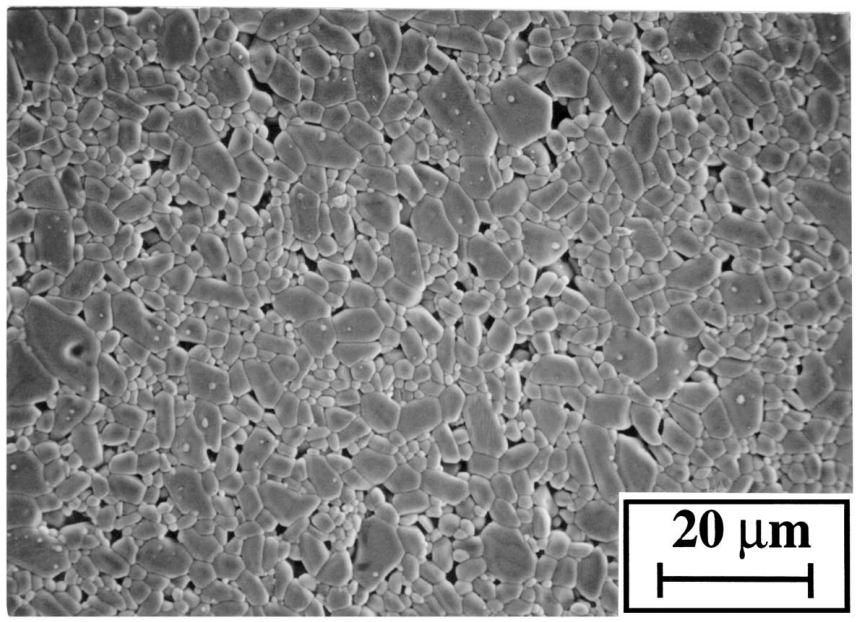

(d)

Figure 15 (*Continued.*)

critical for the process. Therefore, the initial Al particle size should be less than ∼1.5 μm to produce high quality ceramic materials. In addition, it appears to be advantageous to oxidize as much of the Al by solid/gas reaction as possible, and similarly, the solid/gas to liquid/gas ratio should be maximized to obtain dense and defect free ceramic products.

3.2.3. Heating rate

Since the heating rate is one of the processing parameters which can be controlled readily, the effect of the heating rate on the process was investigated by examining the solid-gas reaction range (450–660 °C) at two different heating rates. These heating rates are referred to as fast, 5 °C/min, and slow, 0.5 °C/min. During slow heating the samples were held in the solid state oxidation regime (450–660 °C) for 420 min; however, during fast heating the samples were kept in this temperature regime for only 42 min. The reaction behaviors of fast heat treated and slow heat treated 45B samples are demonstrated in Fig. 16 for 1 h milling time. As seen from these results the fast heating rate results in 11% of the total oxidation in solid state and in slow heating rate this portion is 13%. There is a slight difference between fast and slow heat treated samples. To determine the effect of this small difference on final structure, relative densities of samples were measured and SEM micrographs were taken (Figs 15a and 17A). It is interesting to note that final densities of both samples were identical, $78 \pm 0.5\%$ TD, and their micrographs exhibit similar features such as large pores and flaws. The similar results were obtained for other milling times (i.e., heating rate did not exhibit any significant effect on final microstructures). After 'continuous' heat treatments, the 45B compacts which were prepared by milling for 2, 3, and 4 h were 85, 90, and $94 \pm 0.5\%$ TD, respectively.

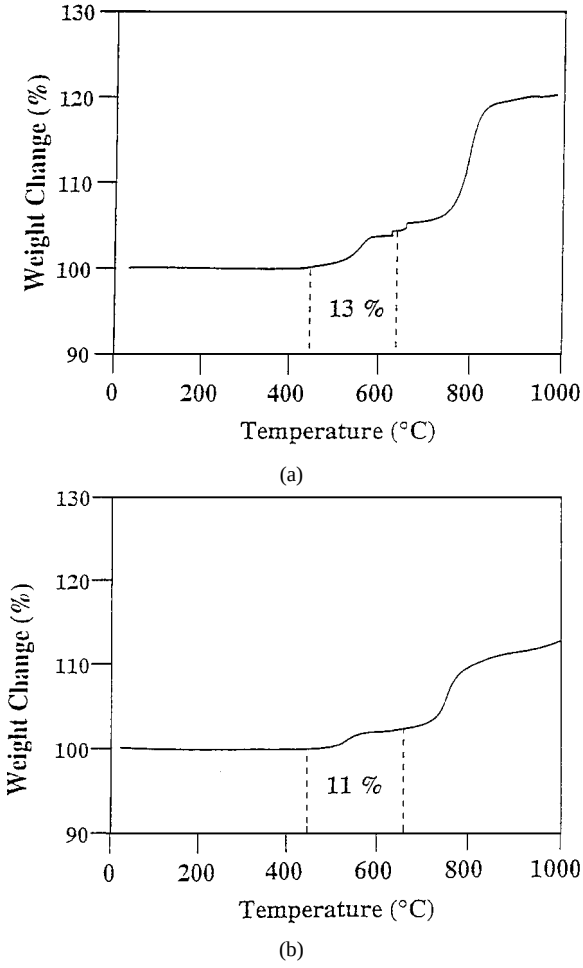

Figure 16 Thermogravimetric analyses of the 45B samples which were compacted at 210 MPa after 1 h milling and heated at (a) 0.5 °C/min and (b) 5 °C/min.

One question was if the samples were held at a temperature for sufficiently long time, would there be a significant effect of the heating rate on the process? Therefore, another set of heat treatment experiments were carried out with the 45B compacts. Samples were heated to 450 or 550 °C at 5 °C/min and held at that temperature for 30 h in air. After this first oxidation step, samples were heated to 1050 °C at 1 °C/min and held at that temperature for 1 h in order to complete the oxidation. All samples were sintered at 1600 °C for 2 h. In order to compare the results from this heat treatment with those from continuous heat treatment, some samples were heated, after the first oxidation, to 650 °C at 1 °C/min and from 650 to 1600 °C at 5 °C/min. These heat treatment experiments could also give an idea about the effect of heating rate on liquid-gas oxidation.

Interestingly, samples exhibited different responses to this heat treatment according to their milling time. After sintering, the 45B compacts that were heat treated at 450 and 550 °C demonstrated similar density values. For example, the 45B compacts with 1, 2, 3, and 4 h milling times which were heat treated at 450 °C exhibited 75, 80, 95, and 97 ± 0.5% TD, respectively. The relative densities for the compacts heat treated at 550 °C were 76, 82, 95 and 97 ± 0.5% TD, respectively. As it can be seen after this heat treatment the samples which were prepared by milling for 1 or 2 h exhibited less amount of densities such as 75 and 80% TD, respectively than the samples that were heat treated by continuous heating (i.e., from room temperature to 1600 °C at 5 °C/min) were 78 and 85% TD. However, samples which were prepared after 3 or 4 h milling demonstrated denser final microstructures (i.e., 95 and 97% TD, respectively) than the samples which were reaction bonded by continuous heating were 90 and 94% TD, respectively. The samples with 97 ± 0.5% TD exhibited 12% linear shrinkage. During these heat treatment experiments solid-gas to liquid-gas ratio was also monitored for each sample. Samples exhibited similar amount of oxidation in solid-gas temperature region. That is, the solid-gas to liquid-gas ratio remained constant. Therefore, the changes in final microstructures

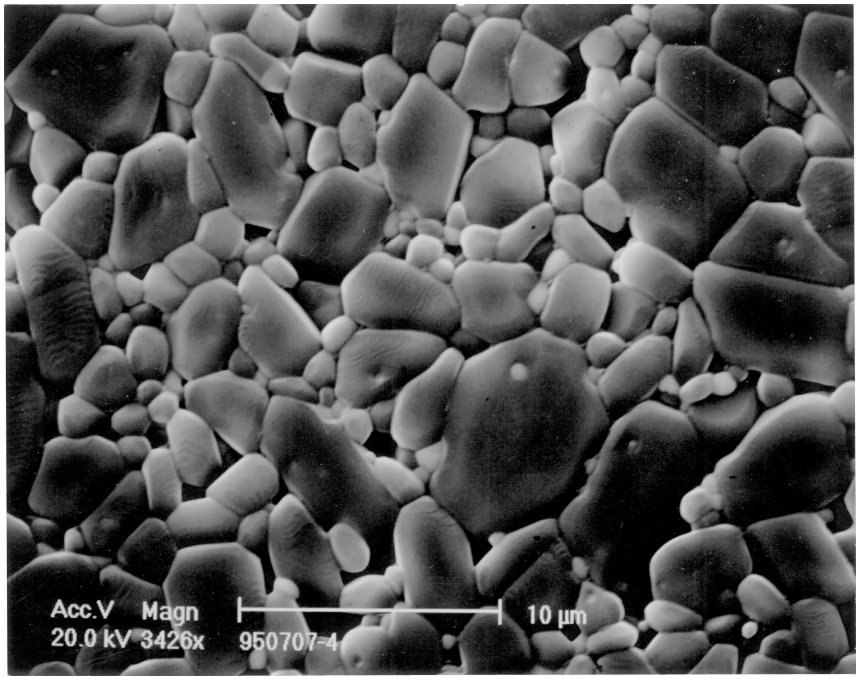

Figure 17 SEM micrographs of the 45B sample which were compacted at 210 MPa after milling for 4 h subjected to isothermal oxidation at 550 °C for 30 h.

can be attributed to the effect of heating rate on liquid-gas oxidation. The differences between responses of samples to the heat treatment may be due to the amount of liquid phase formed during melting.

These results conclude that the one order of magnitude change in heating rate or isothermal oxidation below 660 °C do not change the reaction bonding behavior of Al-alpha alumina particles used in this study. However, heating rate affects the liquid-gas oxidation and slower heating rate during the liquid-gas oxidation improves the final microstructure of samples containing fine Al particles (Fig. 17).

4. Summary and conclusions

During heating of Al + α-Al_2O_3 compacts in air, Al oxidized in the solid state at temperatures <660 °C and in the liquid state at temperatures >660 °C. Below 450 °C the oxidation rate approached zero. Above 450 °C the oxidation rate increased, reaching a maximum at 575 °C for the 1 h milled 45B samples heated at 5 °C/min. It was observed that the amount of solid state oxidation was strongly dependent on the Al particle size. The amount of solid state oxidation relative to the total oxidation were 11 and 34% for the 45B samples which were milled for 1 and 4 h, respectively, heated at 5 °C/min. Due to the initial Al particle size, liquid-gas oxidation exhibited different characteristics. The samples containing large Al particles (>1.5 μm) exhibited two-step liquid-gas oxidation behavior. However, the samples containing fine Al particles (<1.5 μm) demonstrated single step liquid-gas oxidation behavior. At 1200 °C the reaction bonded α-Al_2O_3 started to sinter. The samples from 4 h milled powder, sintered at 1600 °C for 2 h, exhibited 94 ± 0.5% TD with 7% linear shrinkage.

Although the 45A and 60A samples were oxidized completely, the 80A samples exhibited a dense oxide crust and an Al rich core at the end of the reaction bonding stage. These results indicate that large amounts of Al (>60 vol %) are problematic for the reaction bonding process.

It has been shown that large Al particles (>1.5 μm) are detrimental to the reaction bonding process. It was observed that the formation of the liquid phase (molten Al) in the system caused low final relative densities. Therefore, it is always advantageous to oxidize as much Al by solid/gas reaction as possible. It was found that reducing the Al particle size is the most effective way to increase the solid/gas portion in the process.

The heat treatment studies conclude that the one order of magnitude change in heating rate or isothermal oxidation below 660 °C do not change the reaction bonding behavior of Al-alpha alumina particles used in this study. However, heating rate affects the liquid-gas oxidation and slower heating rate during the liquid-gas oxidation improves the final microstructure of samples containing fine Al particles.

As a result of the understanding of the RBAO process which was developed during this study, alpha aluminum oxide ceramics with 97% TD were produced by optimizing the processing parameters such as fine (<1.5 μm) Al particles and slower heating rate during the liquid-gas oxidation.

References

1. M. E. WASHBURN and W. S. COBLENZ, *Amer. Ceram. Soc. Bull.* **67**(2) (1988) 356–363.
2. J. S. HAGGERTY and Y. M. CHIANG, *Ceram. Eng. Sci. Proc.* **11**(7/8) (1990) 757–781.
3. A. J. MOULSON, *J. Mater. Sci.* **14** (1979) 1017–1051.
4. C. W. FORREST, P. KENNEDY and J. V. SHERMAN, in "Ceramics for High Performance Applications," edited by J. J. Burke, A. E. Gorum and R. N. Katz (Brook Hill, Chestnut Hill, MA, 1975) pp. 99–123.
5. M. S. NEWKIRK, A. W. URQUHART, H. R. ZWICKER and E. BREVAL, *J. Mater. Res.* **1**(1) (1986) 81–89.
6. N. CLAUSSEN, T. LE and S. WU, *J. Eur. Ceram. Soc.* **5** (1989) 29–35.
7. N. CLAUSSEN, S. WU and N. A. TRAVITZKY, *Ceram. Eng. Sci. Proc.* **11**(7/8) (1990) 821–841.
8. J. LUYTEN, J. COOYMANS, P. DIELS and J. SLEURS, in "Third Euro-Ceramics," Vol. 1, edited by P. Duran and J. F. Fernandez, 1993, pp. 657–662.
9. J. BRANDT and R. LUNDBERG, in "Third-Euro Ceramics," Vol. 1, edited by P. Duran and J. F. Fernandez, 1993, pp. 169–176.
10. D. E. GARCIA, J. WENDORFF, R. JANSSEN and N. CLAUSSEN, *Ceram. Eng. Sci. Proc.* **15**(5) (1994) 669–676.
11. S. H. YOKOTA, L. C. DE JONGHE and M. N. RAHAMAN, *J. Mater. Sci.* **29** (1994) 4177–4183.
12. J. H. PARK and Z. S. AHN, *J. Mater. Sci. Lett.* **13** (1994) 650–652.
13. S. WU, S. P. GAUS, H. M. CHAN, H. S. CARAM and M. P. HARMER, *Ceramic Transactions* **56** (1995) 209–218.
14. S. WU, D. HOLZ and N. CLAUSSEN, *J. Amer. Ceram. Soc.* **76**(4) (1993) 970–980.
15. N. CLAUSSEN, S. WU and D. HOLZ, *J. Eur. Ceram. Soc.* **14** (1994) 97–109.
16. D. HOLZ, S. WU, S. SCHEPPOKAT and N. CLAUSSEN, *J. Amer. Ceram. Soc.* **77**(10) (1994) 2509–2517.
17. N. SHEHR and J. SCHWEDES, *Ger. Chem. Eng.* **6** (1983) 337–343.
18. K. URABE, A. NAKAJIMA, H. IKAWA and S. UDAGAWA, in "Advances in Ceramics, vol. 24: Science and Technology of Zirconia III," edited by S. Somiya, N. Yamamoto and H. Hanagida (The Amer. Ceram. Soc., Inc., 1988) pp. 345–356.
19. M. J. PRYOR, *Oxidation of Metals* **3**(6) (1971) 523–527.
20. K. WEFERS and C. MISRA, Oxides and hydroxides of aluminum, Alcoa Tech. Paper No. 19, Rev., Alcoa Labs, 1987.
21. V. G. SHEVCHENKO, V. I. KONONENKO, I. N LATOSH, I. A. CHUPOVA and N. V. LUKIN, *Combustion, Explosion and Shock Waves* **30**(5) (1994) 635–637.

Received 7 November 1997
and accepted 10 November 1998